



Available online at [www.sciencedirect.com](http://www.sciencedirect.com)

**ScienceDirect**

Advances in Space Research 63 (2019) 2912–2929

**ADVANCES IN  
SPACE  
RESEARCH**  
(*a COSPAR publication*)  
[www.elsevier.com/locate/asr](http://www.elsevier.com/locate/asr)

# Study of satellite shadow function model considering the overlapping parts of Earth shadow and Moon shadow and its application to GPS satellite orbit determination

Rui Zhang <sup>a,b</sup>, Rui Tu <sup>a,b,c,\*</sup>, Pengfei Zhang <sup>a,c</sup>, Jinhai Liu <sup>a,c</sup>, Xiaochun Lu <sup>a,b,c</sup>

<sup>a</sup> National Time Service Center, Chinese Academy of Sciences, Shu Yuan Road, 710600 Xi'an, China

<sup>b</sup> Key Laboratory of Precision Navigation Positioning and Timing Technology, Chinese Academy of Sciences, Shu Yuan Road, 710600 Xi'an, China

<sup>c</sup> University of Chinese Academy of Sciences, Yu Quan Road, 100049 Beijing, China

Received 29 September 2017; received in revised form 15 January 2018; accepted 2 February 2018

Available online 13 February 2018

## Abstract

Solar radiation pressure is one of the main perturbations in satellite orbit determination. When a satellite enters the umbra or the penumbra area of an occulting body (e.g., the Earth or the Moon), a satellite shadow function model is used to estimate the occultation degree. Occultation of the Sun by the Earth and by the Moon is considered separately in the existing shadow function model, i.e., any area of overlap of the shadows of the Earth and the Moon is not considered. This directly affects the accuracy of the solar radiation pressure model, which then affects the accuracy of satellite orbit determination. In this study, the existing shadow function model was refined to consider the overlap of the shadows of the Earth and the Moon. Then, using the original and refined shadow function models, Global Positioning System (GPS) satellite orbits from 2008 to 2017 were analyzed and compared. The results show that there are 27 occurrences when GPS satellites enter an area of overlapping shadows of the Earth and the Moon. Among them, the longest duration of passage through the overlapping shadows by one satellite in one day is 474 s, and the maximum difference of the same epoch between the original and refined models is 0.329. In addition, Differences between the GPS observed orbits obtained separately using the original and refined models are small. However, differences between the GPS predicted orbits are substantial; the greatest difference is 46 mm. Furthermore, with the reference of overlapping arcs, when there are differences between the predicted orbits obtained separately using the original and refined models, 86.7% of the orbit determination solutions are improved.

© 2018 COSPAR. Published by Elsevier Ltd. All rights reserved.

**Keywords:** Shadow function model; Overlapping shadows; Shadow factor; Observed orbit determination; Predicted orbit determination; Accuracy comparison

## 1. Introduction

For any spacecraft, precise orbit determination is one of the primary requirements for stable operation. For the global navigation satellite system, satellite orbit error is one of the main sources of inaccuracy, which directly affects the

accuracy of navigational positioning. Therefore, the accuracy of satellite orbit determination is of primary concern to the operators and users of navigation systems (Zhang et al., 2015).

An in-orbit satellite is affected by a variety of perturbations, one of the most important of which is solar radiation pressure. A satellite exposed to solar radiation experiences a small force that arises from the absorption or reflection of photons (Montenbruck et al., 2000), which produces the solar radiation pressure perturbation. The acceleration of

\* Corresponding author at: National Time Service Center, Chinese Academy of Sciences, Shu Yuan Road, 710600 Xi'an, China.

E-mail address: [turui-2004@126.com](mailto:turui-2004@126.com) (R. Tu).

an in-orbit satellite caused by solar radiation pressure can be expressed as (Zhang, 2013)

$$\vec{a}_{SR} = \vec{a}_{SRB} + \vec{a}_{SRP}, \quad (1)$$

where  $\vec{a}_{SRB}$  denotes the acceleration of the satellite body caused by the solar radiation pressure perturbation, and  $\vec{a}_{SRP}$  denotes the acceleration of the solar panel caused by the solar radiation pressure perturbation. Parameters  $\vec{a}_{SRB}$  and  $\vec{a}_{SRP}$  can be expressed as

$$\vec{a}_{SRB} = -F\rho_{SR} \left( \frac{1\text{AU}}{\Delta_s} \right)^2 (1 + \eta) \left( \frac{A}{m} \right) \frac{\vec{\Delta}_s}{\Delta_s} \quad (2)$$

and

$$\vec{a}_{SRP} = -F\rho_{SR} \left( \frac{1\text{AU}}{\Delta_s} \right)^2 (1 + \beta) \left( \frac{A_p}{m} \right) \frac{\vec{\Delta}_s}{\Delta_s}, \quad (3)$$

where  $F$  denotes the shadow factor,  $\rho_{SR}$  denotes the constant of solar radiation pressure near the Earth, AU denotes the astronomical unit and 1AU is equal to the average distance between the Sun and the Earth,  $\vec{\Delta}_s$  denotes the vector from the satellite to the Sun,  $\Delta_s$  denotes the distance of  $\vec{\Delta}_s$ ,  $\eta$  denotes the reflectivity coefficient of the satellite body,  $\beta$  denotes the reflectivity coefficient of the solar panel,  $A$  denotes the cross-sectional area of the satellite body normal to the Sun,  $A_p$  denotes the cross-sectional area of the solar panel normal to the Sun and  $m$  denotes the mass of the satellite. Among them,  $F$  can be calculated using the shadow function model. Its main function is to evaluate the degree of occultation of the Sun by the occulting bodies (in this instance, the Earth and the Moon) when a satellite enters the umbra or the penumbra area of the occulting bodies. Accurate calculation of the shadow factor is very important for estimation of the acceleration caused by the solar radiation pressure perturbation.

Many studies have undertaken relevant research on the shadow function model. For example, Montenbruck et al. (2000) proposed a detailed method for solving the satellite shadow function using a conical shadow model. This method has been used widely in orbit determination for the global navigation satellite system. Oraevskii et al. (2004) gave a method of observing the eclipses of the Sun by the Moon from satellite orbits. The conclusions show that the circular orbits with a radius from 50 to 80 thousand kilometers are most efficient for eclipse observations. Based on analyses of the impact of the boundaries of cylindrical and conical shadow models on the orbital integral, Chen (2007) introduced some correcting methods. The conclusions show that based on the correcting methods, the maximal bias of the orbital integration in 3 days length arcs is on centimeter-level, even less. Ding et al. (2010) analyzed the differences between cylindrical and conical shadow models. The conclusions show that the conical shadow model is most suitable for high-precision orbit determination. Mao et al. (2014) analyzed the differences among cylindrical and conical shadow models in eclipse factor

and umbra duration calculation for three types of navigation satellite which includes geostationary Earth orbit (GEO) satellites, inclined geosynchronous orbit (IGSO) satellites, and medium Earth orbit (MEO) satellites. The conclusions show that the calculation error using the cylindrical shadow model for the GEO satellite is larger than for the IGSO and MEO satellites. Srivastava et al. (2015a,b) studied the Earth conical shadow model for low Earth orbit (LEO) satellites and the lunar shadow eclipse prediction models for the Earth orbiting spacecraft. The conclusions show that the results obtained by the oblate Earth conical shadow model is very close to systems tool kit (STK) and the real-time data than the spherical Earth conical shadow models. And, Results obtained by the lunar shadow eclipse prediction models compare well with lunar shadow model given by STK. Based on the spatial view, Du et al. (2016) proposed a satellite shadow model. The conclusions show that the proposed model and the formulae for computing the shadow parameters can provide a prompt profile of the eclipse parameters for medium-high-altitude circular orbit satellites. In summary, recent research on the satellite shadow function model has focused mainly on the establishment of shadow function models and on the influence of these different models on the accuracy of satellite orbit determination. Few studies have considered modeling the method of the satellite shadow function when the shadows of the Sun and the Moon overlap.

According to the mainstream software of GNSS satellite orbit determination, we know that the areas of occultation of the Sun by the Earth and by the Moon are calculated separately in the current processing strategy of the shadow function model. Then, the total occulted area of the Sun is taken as the sum of the separate areas occulted by the Earth and the Moon. When the total occulted area is bigger than the area of the projection disk of the Sun, it is considered that the Sun is completely occulted. However, this processing strategy does not consider the situation when there is overlap of the shadows of the Earth and the Moon (Fig. 1).

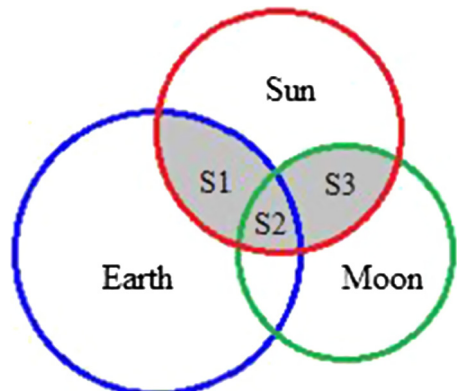


Fig. 1. Illustration of a situation of overlapping Earth and Moon shadows.

As shown in Fig. 1, the area of the Sun occulted by the Earth is  $S_1 + S_2$ , and the area of the Sun occulted by the Moon is  $S_2 + S_3$ . According to the current shadow function model, the total occulted area of the sun is therefore  $(S_1 + S_2) + (S_2 + S_3)$ . However, the correct occulted area should be  $S_1 + S_2 + S_3$ . Therefore, the overlapping shadows of the Earth and the Moon should be considered in practical application.

Based on the above analysis, it is necessary to perfect the current solar radiation pressure model. In this paper, the existing conical shadow function model is presented in Section 2. Then, a refined conical shadow function model that considers the overlapping shadows of the Earth and the Moon is described in Section 3. Based on the Global Positioning System (GPS) final orbit product of the international GNSS service (IGS), the periods of passage of the GPS satellites through the overlapping shadows of the Earth and the Moon are presented in Section 4.1. The differences between the original shadow function model and the refined shadow function model in every overlapping period are given in Section 4.2. Finally, the differences in the accuracy of the GPS orbits obtained separately using the original and refined models are analyzed in Sections 4.3–4.5.

## 2. Conical shadow function model

If the atmosphere and oblateness of an occulting body are ignored, it is sufficient to model occultation using the conical model. The conical shadow function model of the occultation of the Sun by the Earth is shown in Fig. 2.

It can be seen from Eqs. (2) and (3) and Fig. 2 that the value of the shadow factor can be divided into the following three cases:

- (a) The satellite can receive all the sunlight from the sun; at this time  $F = 1$ .
- (b) The satellite is in the penumbra area of the Earth and it can receive only part of the sunlight from the Sun; at this time  $0 < F < 1$ .
- (c) The satellite is in the umbra area of the Earth and it cannot receive any sunlight from the Sun; at this time  $F = 0$ .

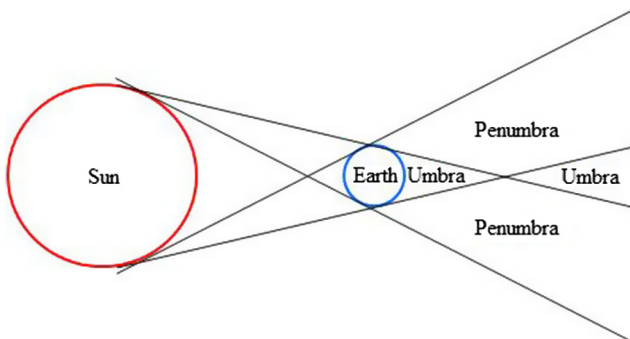


Fig. 2. Conical shadow function model of the occultation of the Sun by the Earth.

Because of the small apparent diameter of the Sun, it is sufficient to model occultation using overlapping circular disks (Montenbruck et al., 2000). First, two concepts are introduced:

- (a) Apparent radius: this refers to the angle between the connection from the eyes of an observer to the center of the arc and the tangent from the eyes of an observer to the arc.
- (b) Apparent separation: this refers to the angle between the connections from the eyes of an observer to the centers of two arcs.

The relationship between the satellite, Earth, and Sun is shown in Fig. 3.

As shown in Fig. 3, the apparent radius of the Earth can be expressed as

$$\theta_e = \arcsin \frac{R_e}{|\mathbf{r}|}, \quad (4)$$

where  $R_e$  denotes the radius of the Earth and  $\mathbf{r}$  denotes the position vector of the satellite in the geocentric coordinate system. The apparent radius of the Sun can be expressed as

$$\theta_s = \arcsin \frac{R_s}{|\mathbf{r}_s - \mathbf{r}|}, \quad (5)$$

where  $R_s$  denotes the radius of the Sun and  $\mathbf{r}_s$  denotes the position vector of the Sun in the geocentric coordinate system. The apparent separation between the Earth and the Sun can be expressed as

$$\theta_{es} = \arccos \frac{-\mathbf{r}^T(\mathbf{r}_s - \mathbf{r})}{|\mathbf{r}||\mathbf{r}_s - \mathbf{r}|}. \quad (6)$$

When the satellite is in the penumbra area, the calculation method of the shadow function is as shown in the following.

First, the occulting body (such as the Earth) and the Sun are projected in the direction of satellite sight (Fig. 4).

As shown in Fig. 4,  $AC$  represents the apparent radius of the Sun,  $BC$  represents the apparent radius of the Earth, and  $AB$  represents the apparent separation between the Sun and the Earth. The part shaded gray is the part of the Sun occulted by the occulting body. It can be calculated

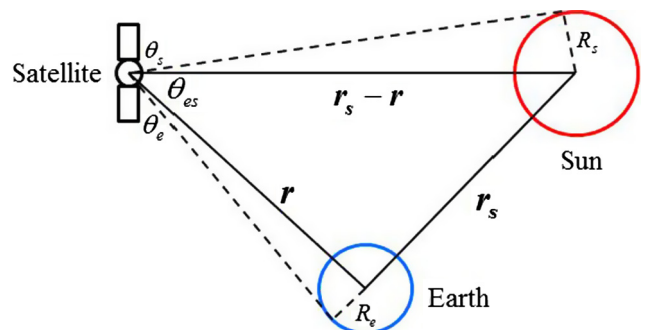


Fig. 3. Illustration of apparent radius and apparent separation.

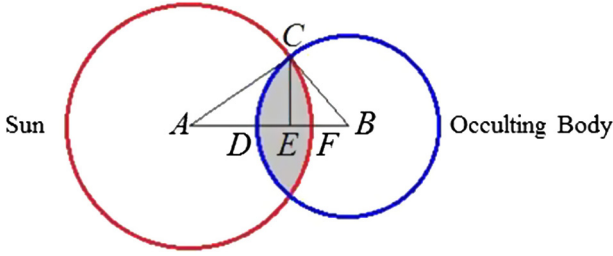


Fig. 4. Illustration of occultation of the Sun by an occulting body.

by adding the areas of the two arches that are separated by the common chord of the two projection disks. Therefore, the occulted area can be expressed as

$$S = 2(S_{AFC} - S_{AEC}) + 2(S_{BDC} - S_{BEC}), \quad (7)$$

where

$$S_{AFC} = \frac{1}{2} \cdot \angle CAF \cdot \theta_s^2, \quad (8)$$

$$S_{AEC} = \frac{1}{2} \cdot (\theta_s \cdot \sin \angle CAF) \cdot (\theta_e \cdot \cos \angle CAF), \quad (9)$$

$$S_{BDC} = \frac{1}{2} \cdot \angle CBD \cdot \theta_e^2, \quad (10)$$

and

$$S_{BEC} = \frac{1}{2} \cdot (\theta_e \cdot \sin \angle CBD) \cdot (\theta_e \cdot \cos \angle CBD). \quad (11)$$

In Eqs. (8) and (10),

$$\angle CAF = \arccos \frac{\theta_s^2 + \theta_{es}^2 - \theta_e^2}{2\theta_s\theta_{es}} \quad (12)$$

and

$$\angle CBD = \arccos \frac{\theta_e^2 + \theta_{es}^2 - \theta_s^2}{2\theta_e\theta_{es}}. \quad (13)$$

The shadow factor is thus given by

$$F = 1 - \frac{S}{\pi\theta_s^2}. \quad (14)$$

When there is only one occulting body, whether the Sun is occulted by the Earth can be judged by  $\theta_e$ ,  $\theta_s$ , and  $\theta_{es}$ . When  $\theta_{es} \geq \theta_e + \theta_s$ , occultation does not take place; when  $\theta_{es} \leq \theta_e - \theta_s$ , occultation is total; and when  $\theta_{es} \leq \theta_s - \theta_e$  or  $|\theta_e - \theta_s| < \theta_{es} < \theta_e + \theta_s$ , occultation is partial. The calculation processing of the shadow function is as illustrated in Fig. 5.

### 3. Satellite shadow function model considering the overlapping shadows of the Earth and the Moon

When the Sun is occulted by the Earth and by the Moon concurrently, the shadows of the Earth and the Moon might overlap. There could be various overlapping situations (Fig. 6).

Irrespective of the overlapping situation, the total occulted area of the Sun can be expressed as

$$S = S_e + S_m - S_{public}, \quad (15)$$

where  $S$  denotes the total area of the Sun occulted by the Earth and by the Moon,  $S_e$  denotes the area of the Sun occulted by the Earth,  $S_m$  denotes the area of the Sun occulted by the Moon, and  $S_{public}$  denotes the common area of the Sun occulted by the Earth and by the Moon. The values of  $S_e$  and  $S_m$  can be obtained using the calculation method outlined in Section 2. The main problem to be solved is how to calculate the area of the common occulted part.

Before performing the calculation, the following known values can be obtained using the calculation method presented in Section 2: i.e., the apparent radius of the Earth  $\theta_e$ , apparent radius of the Moon  $\theta_m$ , apparent radius of the Sun  $\theta_s$ , apparent separation between the Earth and the Sun  $\theta_{es}$ , apparent separation between the Earth and the Moon  $\theta_{em}$ , and apparent separation between the Moon and the Sun  $\theta_{ms}$ . In special cases, the Moon will be in the umbra area of the Earth or the Earth will be in the umbra area of the Moon. Although the shadows of the Earth and the Moon overlap at this time, the occultation of the Sun can be expressed as the area occulted by the Earth or by the Moon directly. Except for these two situations, the processing method of the general overlapping situation (Fig. 7) is as follows.

As shown in Fig. 7, the overlapping part can be divided into at most one polygon and several arches. The area of the overlapping parts of the Earth and the Moon shadows can be expressed as

$$S_{public} = \begin{cases} 0, n = 0 \\ \sum_{i=1}^n S_{ai}, n = 2 \\ S_p + \sum_{i=1}^n S_{ai}, n \geq 3 \end{cases}, \quad (16)$$

where  $S_p$  denotes the area of the polygon that is surrounded by the overlapping part,  $S_{ai}$  denotes the area of the arch corresponding to each edge of the polygon in the corresponding projection circle, and  $n$  denotes the number of intersections of the projection circles in the overlapping part.

Taking into account the problem of program implementation, the model should automatically identify a variety of overlapping situations. In this paper, the Earth, Moon, and Sun are projected to a plane from the direction of the satellite sight and a plane Cartesian coordinate system is constructed. Then, the overlapping situation is determined automatically through the method of plane geometry. Considering the symmetry of the overlapping situation, the method of construction of the plane Cartesian coordinate system is shown in Fig. 8.

In the plane Cartesian coordinate system, the origin is the center of the projection circle of the Earth. The x-axis points to the center of the projection circle of the Moon, and the y-axis completes the right-handed coordinate sys-

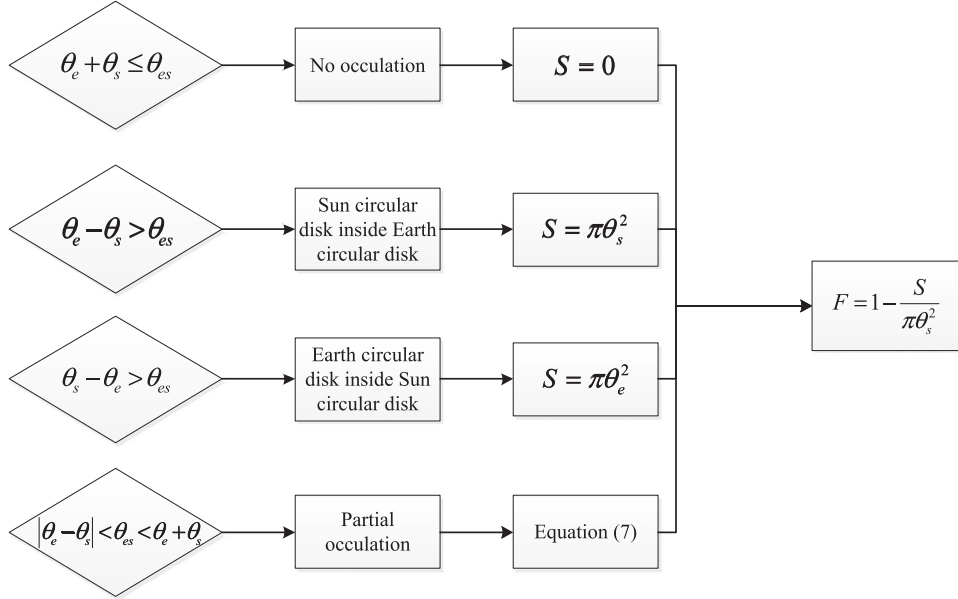


Fig. 5. Calculation process of the shadow function when there is only one occulting body.

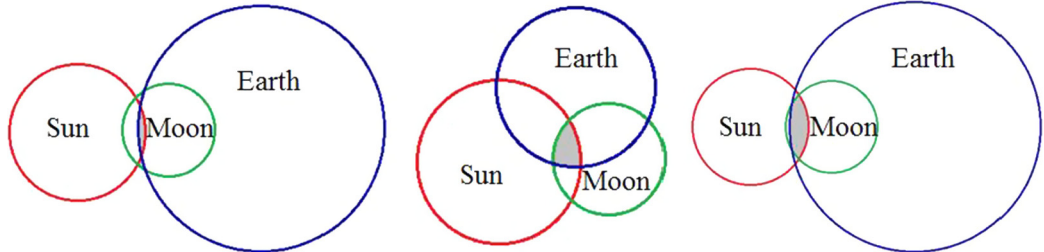


Fig. 6. Illustration of several overlapping situations.

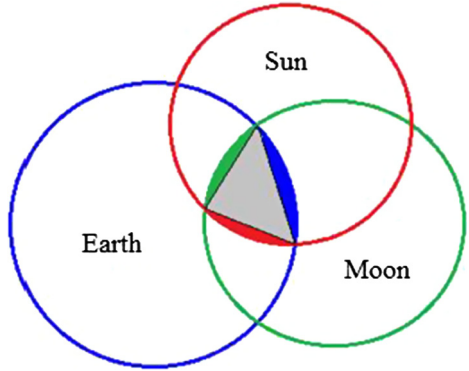


Fig. 7. Illustration of the general overlapping situation.

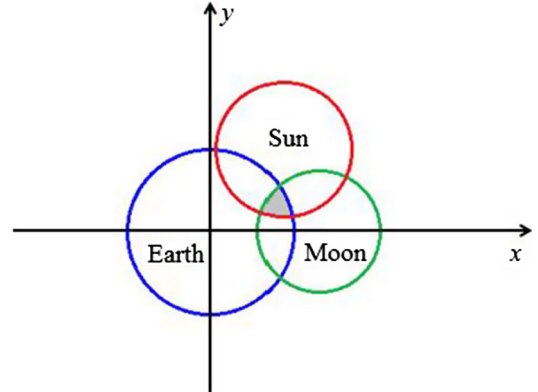


Fig. 8. Illustration of the method of construction of the plane Cartesian coordinate system.

tem. According to the plane Cartesian coordinate system, the coordinate of the center of the projection circle of the Earth can be expressed as

$$x_e = 0, y_e = 0, \quad (17)$$

the coordinate of the center of the projection circle of the Moon can be expressed as

$$x_e = \theta_{em}, y_e = 0, \quad (18)$$

and the coordinate of the center of the projection circle of the Sun can be expressed as

$$x_s = \theta_{es} \cdot \frac{\theta_{es}^2 + \theta_{em}^2 - \theta_{ms}^2}{2 \cdot \theta_{es} \cdot \theta_{em}}, y_s = \sqrt{\theta_{es}^2 - x_s^2}. \quad (19)$$

It can be seen from Eq. (16) that it is necessary to determine the number of intersections of the overlapping part before calculating its area. In this paper, the coordinates of the intersections of the three projection circles are calculated first. Then, by establishing whether the distance of the intersection of any two projection circles to the center of the third projection circle is less than or equal to the radius of the third projection circle, it is determined whether this intersection is in the overlapping part.

For the intersections of the projection circles of the Earth and the Moon, according to the coordinate system, the two intersections are symmetrical about the x-axis. Therefore, the coordinates of the two intersections can be expressed as

$$x_{em1} = \theta_e \cdot \frac{\theta_e^2 + \theta_{em}^2 - \theta_m^2}{2 \cdot \theta_e \cdot \theta_{em}}, \quad y_{em1} = \sqrt{\theta_e^2 - x_{em1}^2} \quad (20)$$

and

$$x_{em2} = \theta_e \cdot \frac{\theta_e^2 + \theta_{em}^2 - \theta_m^2}{2 \cdot \theta_e \cdot \theta_{em}}, \quad y_{em2} = -\sqrt{\theta_e^2 - x_{em2}^2}. \quad (21)$$

When calculating the coordinates of the intersections of the projection circles of the Earth and the Sun, for simplicity, the plane Cartesian coordinate system can be first rotated (Fig. 9) to calculate the coordinates of the intersections in a new coordinate system. Then, the rotation matrix can be used to obtain the coordinates of the intersections in the original coordinate system.

As shown in Fig. 9, the rotation angle of the two coordinate systems can be expressed as

$$\eta_{es} = \arccos \frac{x_s}{\theta_{es}}. \quad (22)$$

The coordinates of the two intersections in the rotated coordinate system can be expressed as

$$x'_{es1} = \theta_e \cdot \frac{\theta_e^2 + \theta_{es}^2 - \theta_s^2}{2 \theta_e \theta_{es}}, \quad y'_{es1} = \sqrt{\theta_e^2 - x'_{es1}^2} \quad (23)$$

and

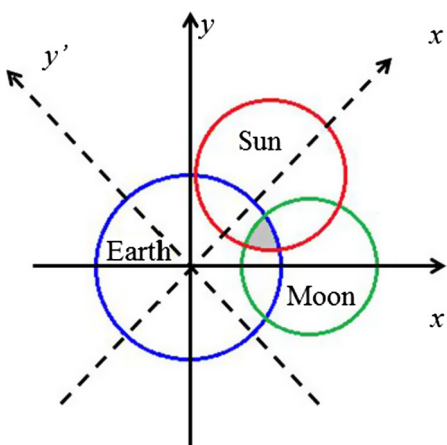


Fig. 9. Illustration of the rotation of the coordinate system.

$$x'_{es2} = \theta_e \cdot \frac{\theta_e^2 + \theta_{es}^2 - \theta_s^2}{2 \theta_e \theta_{es}}, \quad y'_{es2} = -\sqrt{\theta_e^2 - x'_{es2}^2}. \quad (24)$$

Then, the coordinates of the intersections of the projection circles of the Earth and the Sun can be expressed as

$$x_{es1} = x'_{es1} \cdot \cos \eta_{es} - y'_{es1} \cdot \sin \eta_{es},$$

$$y_{es1} = x'_{es1} \cdot \sin \eta_{es} + y'_{es1} \cdot \cos \eta_{es} \quad (25)$$

and

$$x_{es2} = x'_{es2} \cdot \cos \eta_{es} - y'_{es2} \cdot \sin \eta_{es},$$

$$y_{es2} = x'_{es2} \cdot \sin \eta_{es} + y'_{es2} \cdot \cos \eta_{es}. \quad (26)$$

Similarly, when calculating the coordinates of the intersections of the projection circles of the Moon and the Sun, the plane Cartesian coordinate system can be first rotated and translated (Fig. 10).

As shown in Fig. 10, the rotation parameter  $\eta_{ms}$  and the translation parameter  $l_{ms}$  can be expressed as

$$\eta_{ms} = \arccos \frac{x_s - x_m}{\theta_{ms}} \quad (27)$$

and

$$l_{ms} = \theta_{em}. \quad (28)$$

The coordinates of the two intersections in the new coordinate system can be expressed as

$$x'_{ms1} = \theta_m \cdot \frac{\theta_m^2 + \theta_{ms}^2 - \theta_s^2}{2 \theta_m \theta_{ms}}, \quad y'_{ms1} = \sqrt{\theta_m^2 - x'_{ms1}^2} \quad (29)$$

and

$$x'_{ms2} = \theta_m \cdot \frac{\theta_m^2 + \theta_{ms}^2 - \theta_s^2}{2 \theta_m \theta_{ms}}, \quad y'_{ms2} = -\sqrt{\theta_m^2 - x'_{ms2}^2}. \quad (30)$$

Then, the coordinates of the intersections of the projection circles of the Moon and the Sun can be expressed as

$$x_{ms1} = x'_{ms1} \cdot \cos \eta_{ms} - y'_{ms1} \cdot \sin \eta_{ms} + l_{ms},$$

$$y_{ms1} = x'_{ms1} \cdot \sin \eta_{ms} + y'_{ms1} \cdot \cos \eta_{ms} \quad (31)$$

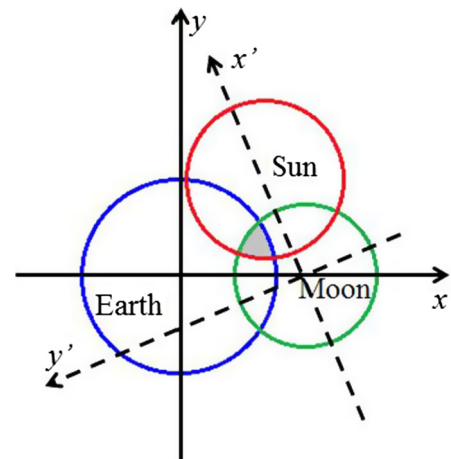


Fig. 10. Illustration of the rotation and translation of the coordinate system.

and

$$\begin{aligned} x_{ms2} &= x'_{ms2} \cdot \cos \eta_{ms} - y'_{ms2} \cdot \sin \eta_{ms} + l_{ms}, \quad y_{ms2} \\ &= x'_{ms2} \cdot \sin \eta_{ms} + y'_{ms2} \cdot \cos \eta_{ms}. \end{aligned} \quad (32)$$

After determining the number of intersections in the overlapping part, the area of the overlapping part can be calculated by different algorithms according to Eq. (16). When the number of intersections is  $>2$ , a polygon can be surrounded in the overlapping part, and the area of this polygon can be obtained using the following equation:

$$S_p = \frac{1}{2} \sum_{i=1}^n (x_i y_{i+1} - x_{i+1} y_i) \quad (x_{n+1} = x_1, y_{n+1} = y_1), \quad (33)$$

where  $(x_i, y_i)$  denotes the coordinates of the vertices of the polygon. However, as a condition, the vertices must be arranged in a specific sequence. As shown in Fig. 11, the order of the vertices should be a–b–c–d–a (right), rather than a–c–d–b–a (left).

In a plane Cartesian coordinate system, for any linear function  $y = ax + b$ , when a number of points all meet the condition  $y_i > ax_i + b$  or the condition  $y_i < ax_i + b$ , it is proven that these points are on the same side of the line that corresponds to the linear function. According to this theory, the vertices of the polygon in the overlapping part can be ordered. First, one point  $(x_1, y_1)$  is chosen as the first point. Then, the first point is connected to another point to constitute a linear function. If the remaining points, other than the two selected points are on the same side of the line that corresponds to the linear function, the second point  $(x_2, y_2)$  is determined. Otherwise, the first point is connected to another point and so on until the second point is determined. After the second point is determined, the second point is used as the starting point and the method is repeated. This method is used until the order of all the points is determined.

The area of the arch that corresponds to each edge of the polygon should be calculated after determining the polygon area. The area of the arch can be obtained by subtracting the area of a triangle from the area of a sector. When calculating the area of the arch, the first thing is to determine in which projection circle the arch is located. Then, it is necessary to determine which of the two arches separated by the edge in the projection circle is in the overlapping area. As shown in Fig. 12, it is necessary to establish which arch is in the overlapping part, the  $a1$  side or the  $a2$  side.

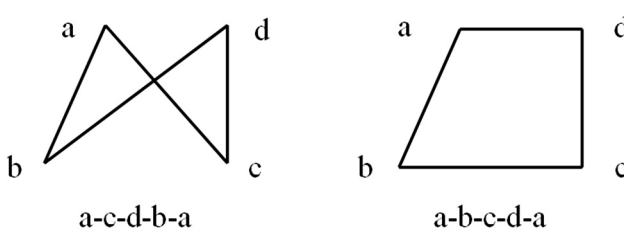


Fig. 11. Illustration of the order of vertices of the polygon.

As shown in Fig. 12,  $a1$  and  $a2$  are the intersections of the vertical diameter of edge and the circle. Judging which intersection is in the three projection circles at the same time can determine which side of the arch is in the overlapping area. In general, the two intersections of the vertical diameter of edge and the circle can be expressed as

$$x_{a1} = x + r \cdot \cos \alpha, \quad y_{a1} = y + r \cdot \sin \alpha \quad (34)$$

and

$$x_{a2} = x - r \cdot \cos \alpha, \quad y_{a2} = y - r \cdot \sin \alpha, \quad (35)$$

where  $(x, y)$  denotes the center coordinates of the projection circle that corresponds to the edge,  $r$  denotes the radius of the circle that corresponds to the edge, and  $\alpha$  denotes the inclination of the edge. The inclination can be expressed as

$$\alpha = \begin{cases} \beta & (\beta \geq 0) \\ \beta + \pi & (\beta < 0) \end{cases}, \quad (36)$$

where

$$\beta = \arctan \left( -\frac{x_2 - x_1}{y_2 - y_1} \right), \quad (37)$$

where  $(x_1, y_1)$  and  $(x_2, y_2)$  denote the coordinates of the two endpoints of the edge. In particular, when  $y_1 = y_2$ , the two intersections of the vertical diameter of edge and the circle can be expressed as

$$x_{a1} = x, \quad y_{a1} = y + r \quad (38)$$

and

$$x_{a2} = x, \quad y_{a2} = y - r. \quad (39)$$

Using the two endpoints of the edge and the judged intersection of the vertical diameter of edge and the circle  $(x_a, y_a)$ , the area of the arch can be expressed as

$$S_a = \frac{1}{2} \varphi \cdot r^2 - \frac{1}{2} r \cdot dist_2 \cdot \cos \left( \frac{1}{2} \varphi \right), \quad (40)$$

where

$$\varphi = 2 \arccos \left( \frac{2r^2 - dist_1^2}{2r^2} \right), \quad (41)$$

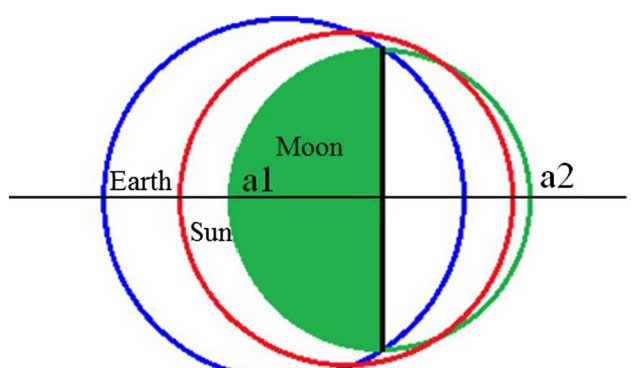


Fig. 12. Illustration of the determination of the arch in the overlapping area.

$$dist_1 = \sqrt{(x_a - x_1)^2 + (y_a - y_1)^2}, \quad (42)$$

and

$$dist_2 = \sqrt{(x_2 - x_1)^2 + (y_2 - y_1)^2}. \quad (43)$$

After obtaining the area of each arch, the area of the overlapping part can be obtained using Eq. (16). Then, the occulted area of the Sun can be calculated using Eq. (15) when there is overlap of the shadows of the Earth and the Moon. Finally, the shadow factor can be obtained using Eq. (14).

In the actual data process, the areas of the Sun occulted by the Earth and by the Moon are first calculated separately using the method of Section 2. Then, if there is overlap of the shadows of the Earth and the Moon, the shadow factor considering the overlapping part can be obtained by the method of Section 3. The specific calculation process is shown in Fig. 13.

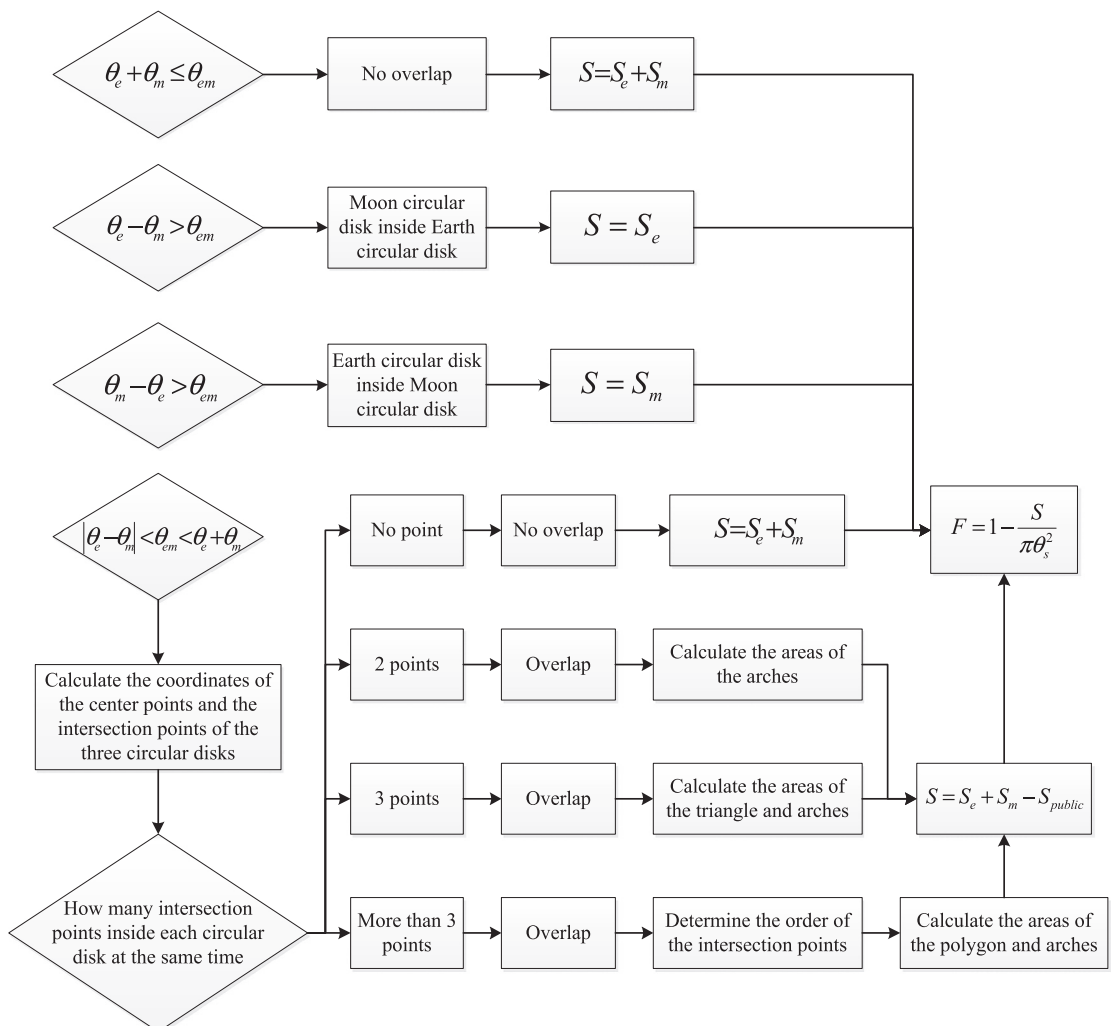


Fig. 13. Calculation process of the shadow factor when there is overlap of the shadows of the Earth and the Moon.

## 4. Numerical experiment

### 4.1. Statistics of periods of overlapping shadows of the Earth and the Moon

The dynamics parameters of each day of each GPS satellite from January 2008 to May 2017 were obtained using the GPS final orbit products of IGS. Then, based on the satellite shadow function model and considering the overlapping shadows of the Earth and the Moon, the orbital integral method was used to select the time at which the GPS satellite entered the area of overlapping shadows of the Earth and the Moon. Among them, in order to select the time more accurately, the integral step was set to 1 s. The models and the strategies of the orbital integral method are shown in Table 1. The details of the GPS satellites passed through the overlapping shadows of the Earth and the Moon are shown in Table 2.

Table 1

Models and strategies of the orbital integral method.

Item	Models and strategies
Integral step	1 s
Earth gravity	EIGEN (Förste et al., 2011) up to $12 \times 12$
N-body	JPL DE405 (Standish, 1998)
Tide displacement	IERS conventions 2010 (Petit et al., 2010), FES2004 (Lyard et al., 2006)
Solar radiation	5 BERN parameters (Beutler et al., 1994; He et al., 2013; Lou et al., 2014)
Atmosphere drag	Not considered
Relativity	IERS conventions 2010 (Petit et al., 2010)
Earth radiation	Considered
Integration method	Runge-Kutta single-step integration method and Adams multi-step integration method (Montenbruck et al., 2000; Dai, 2016)

It can be seen from Table 2 that according to the refined shadow function model and the GPS final orbit products, from January 2008 to May 2017, the GPS satellites enter the area of overlapping shadows of the Earth and the Moon 27 times. Among them, five satellites (G12, G16, G20, G25, and G28) in the B orbital plane enter the area of overlapping shadows 16 times. The highest number of times a satellite entered the overlapping area is six (G16). The longest duration of passage through the overlapping shadows in one day (474 s) and the greatest number of epochs for which the orbital integral is affected (8) are for G12 on day of year (DOY) 079 2015.

#### 4.2. Comparison of shadow factor

The 27 overlapping periods selected in Section 4.1 were analyzed to compare the differences of the shadow factors obtained separately using the original and refined shadow function models. The compared results of the shadow factors of each epoch in every overlapping period are shown in Fig. 14. The maximum values of the differences of the shadow factors in every overlapping period are shown in Fig. 15. Considering each duration of passage through the overlapping shadows is different, in order to reflect the law of change of the shadow factor with a more clearly resolution, the scale of each horizontal axis is different in Fig. 14.

Table 2

Details of GPS satellite passage through the area of overlapping shadows of the Earth and the Moon.

Serial number	PRN	Year	Doy	Start time (sod)	End time (sod)	Duration (s)	Number of orbital integral epochs in overlapping period (sampling interval: 60 s)
1	G16	2008	038	18,412	18,471	59	1
2	G16	2008	214	39,128	39,195	67	1
3	G28	2009	026	33,518	33,596	78	1
4	G23	2010	015	24,985	25,067	82	1
5	G12	2010	192	70,255	70,334	79	2
6	G25	2010	192	71,020	71,104	84	2
7	G30	2010	192	73,467	73,561	94	2
8	G13	2011	004	27,809	27,958	149	5
				28,671	28,826	155	
9	G28	2011	004	35,097	35,155	58	1
10	G12	2011	152	72,674	72,743	69	1
11	G22	2011	152	79,217	79,298	81	1
12	G25	2011	152	76,222	76,300	78	1
13	G14	2011	182	32,012	32,016	4	0
14	G20	2011	329	26,241	26,375	134	2
15	G32	2011	329	24,631	24,695	64	1
16	G32	2012	142	2924	3015	91	2
17	G05	2012	318	83,827	83,878	51	2
				85,281	85,396	115	
18	G18	2013	307	51,873	51,988	115	2
19	G28	2014	119	16,179	16,208	29	1
20	G12	2015	079	30,237	30,457	220	8
				30,804	31,058	254	
21	G25	2015	079	33,542	33,649	107	1
22	G16	2015	256	23,863	24,121	258	5
23	G04	2016	068	86,011	86,053	42	1
24	G16	2016	069	3715	3795	80	2
25	G16	2016	245	25,152	25,208	56	1
26	G03	2017	057	51,382	51,466	84	1
27	G16	2017	057	46,063	46,094	31	1

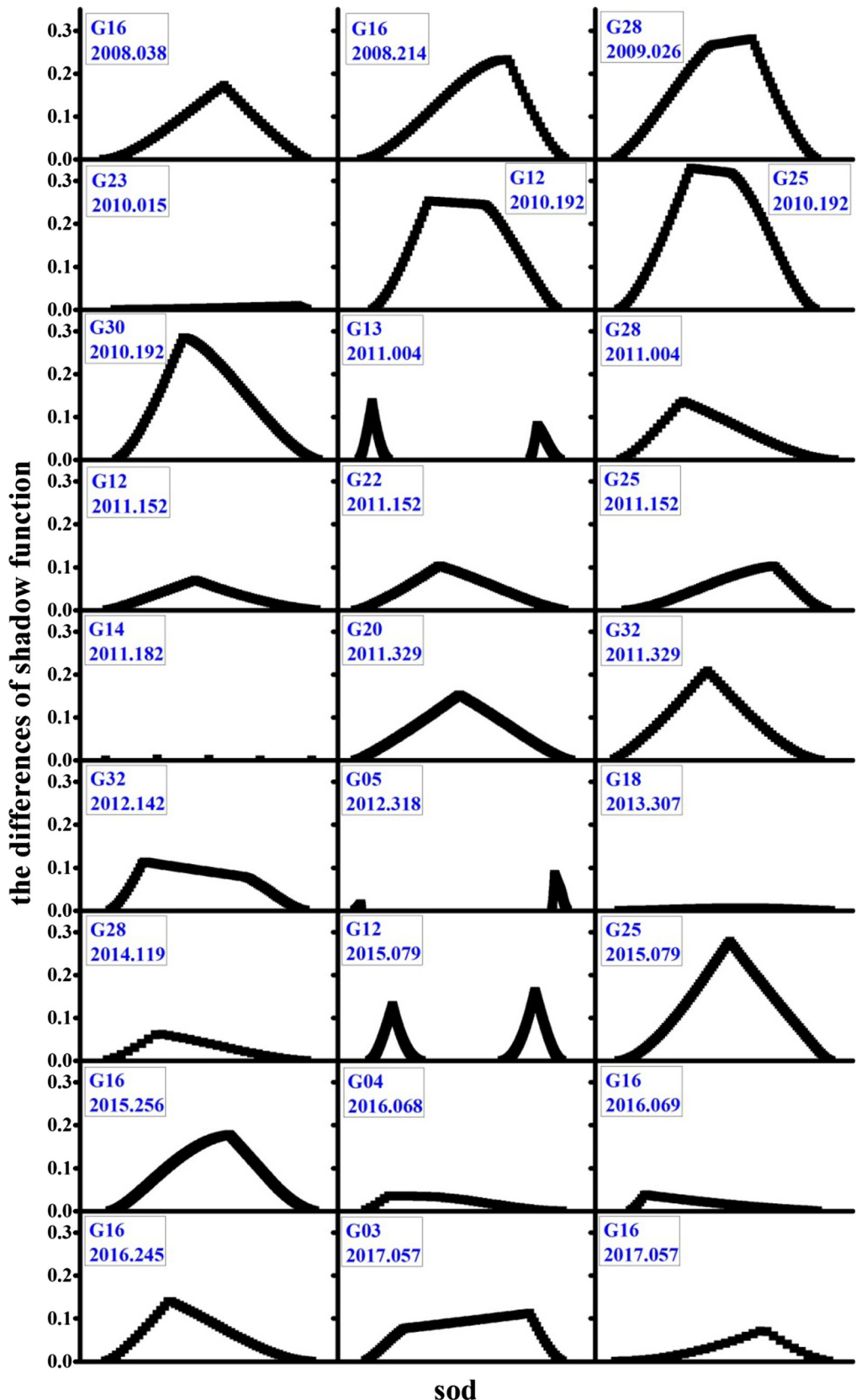


Fig. 14. Comparisons of the shadow factors of each epoch in every overlapping period.

It can be seen from Fig. 14 that in a continuous overlapping period, the differences of the shadow factors

obtained using the original and refined shadow function models increase gradually from a value close to zero to

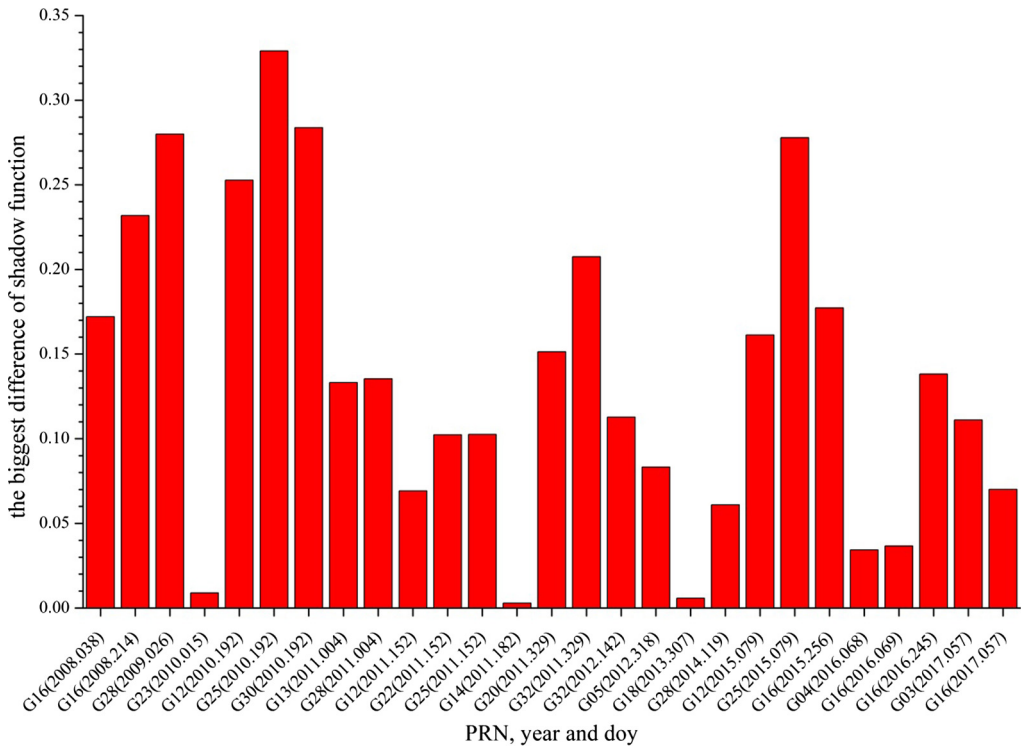


Fig. 15. Maximum values of the differences of the shadow factors in every overlapping period.

the maximum value and then decrease gradually to a value close to zero. As shown in Fig. 15, the maximum value of the difference of the shadow factor (0.329) was for G25 of DOY 192 2010. This difference is close to 1/3 of the solar radiation pressure perturbation. It is therefore necessary to consider the overlap of the shadows of the Earth and the Moon in the satellite shadow function model.

#### 4.3. Comparison of GPS orbit determination

To analyze the influence of the refined shadow function model on orbit determination, the GPS satellite orbits were obtained separately using the original and the refined shadow function models. Then, the results of the orbit determinations were compared. The following three schemes were used and the illustration is shown in Fig. 16.

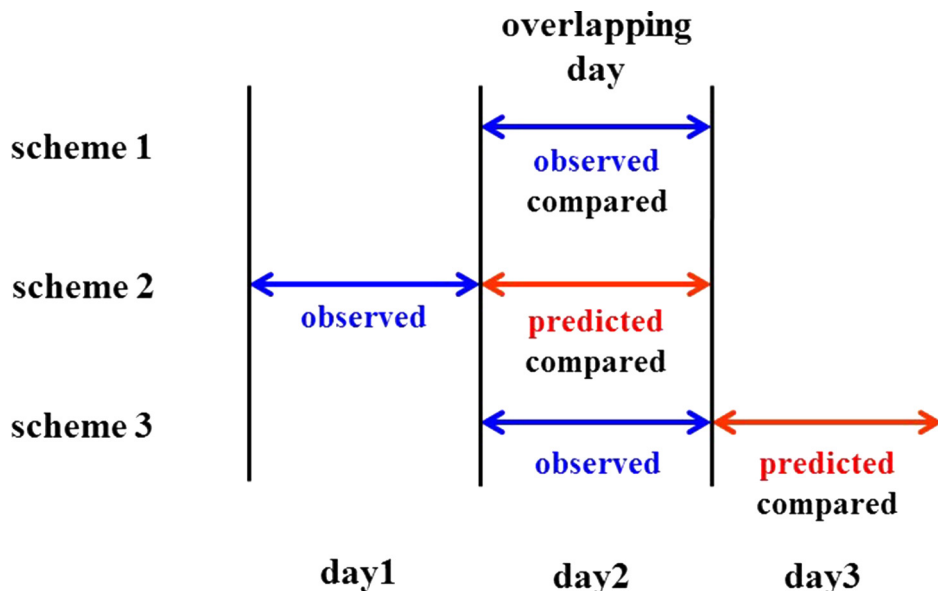


Fig. 16. Illustration of scheme1, scheme 2, and scheme 3.

Table 3

Models and strategies of the data processing.

Item	Models and strategies
Integral step	60 s
Observation equation method	Undifferenced (Tu et al., 2013a; Tu et al., 2013b)
Observations	Ionosphere-free code and phase combined observations
Sampling rate of data preprocessing	30 s
Sampling rate of parameter estimation	300 s
Cut-off elevation	7°
Station coordinate	Estimated in entire arc
Satellite clock error	Estimated in every epoch
Receiver clock error	Estimated in every epoch
Tropospheric delay	Estimated in 1-h arc
Earth rotation parameter	Estimated in entire arc (EOPs published by IERS were used as the a priori ERPs and they were constrained heavily)
Velocity breaks parameters	Not estimated (Under the situation with the actual force, the impact of the refined model on the accuracy of orbit determination can be reflected more accurately. Therefore, the experience compensation was not used in this paper.)
Ambiguity	Fixed (Using double difference observations)
Satellite phase center	igs08.atx
Station phase center	igs08.atx

Scheme 1: the observed orbits of the overlapping day were calculated and compared.

Scheme 2: the observed orbits of the day before the overlapping day were calculated and predicted orbits predicted for the overlapping day. Then, the predicted orbits were compared.

Scheme 3: the observed orbits of the overlapping day were calculated and predicted orbits predicted for the day after the overlapping day. Then, the predicted orbits were compared.

The tracking stations used in the orbit determination of each day were as far as possible the same as the station list

of the IGS final clock product of the same day. The three-dimensional coordinates and the priori accuracy of the IGS tracking stations was obtained from the IGS site coordinates product (indicated by SNX) (Dow et al., 2009) for the corresponding GPS week. The orbital integral models and strategies were the same as in Table 1 except for the orbital integral step. The models and strategies of data processing are shown in Table 3. The comparisons of the GPS orbit determination solutions of the three schemes are shown in Fig. 17.

It can be seen from Fig. 17 that the differences of the observed orbits obtained by scheme 1 are small, i.e., typically, they are within 1 mm and the largest difference is 2

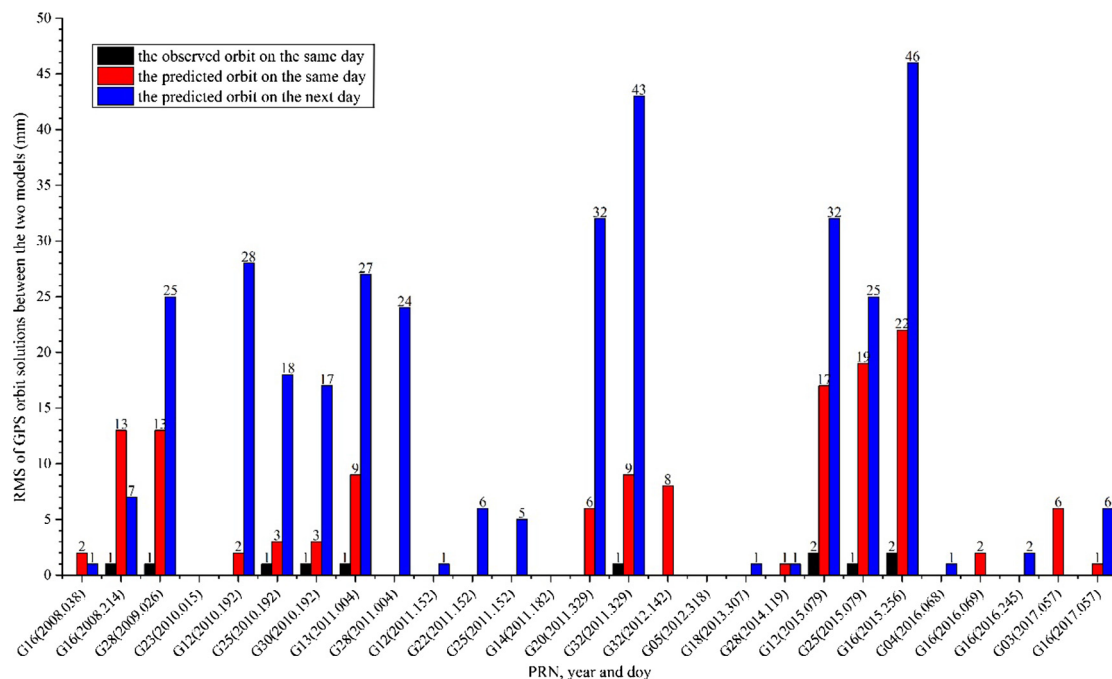


Fig. 17. Comparisons of the GPS orbit determination solutions of the three schemes.

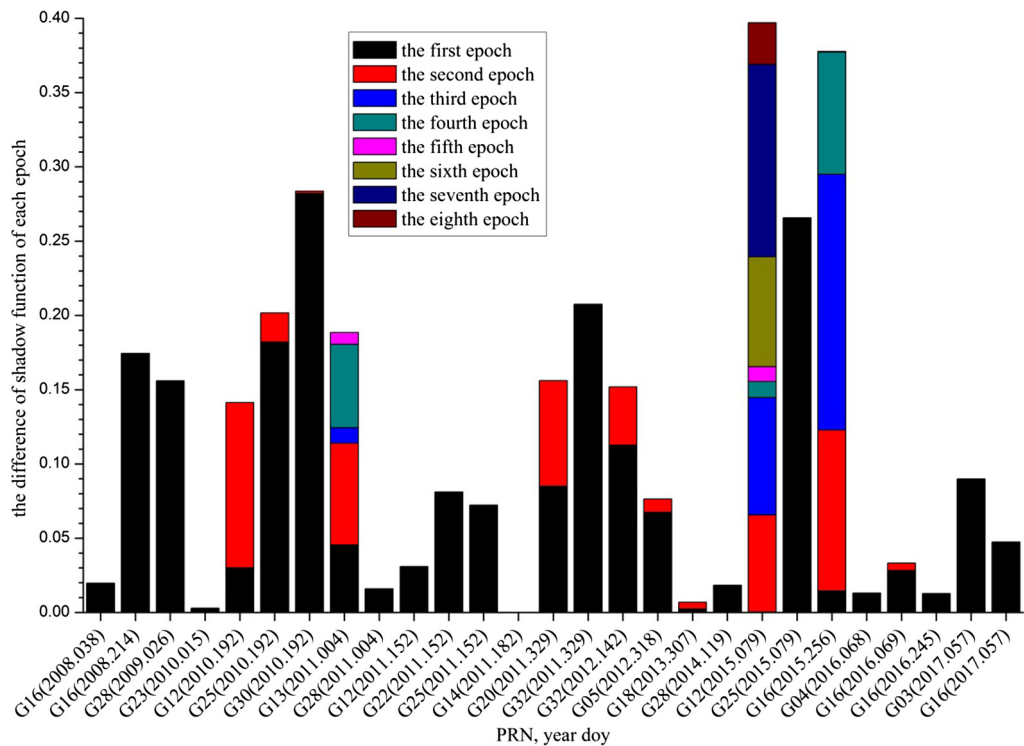


Fig. 18. Cumulative differences of the shadow factors at the orbital integral epochs in every overlapping period.

mm. However, the differences of the predicted orbits obtained by schemes 2 and 3 are larger, and the differences of the predicted orbits obtained by scheme 3 are bigger than scheme 2. The maximum difference of 24-h predicted orbit is 46 mm. This is mainly because the observed orbit is constrained by the full arc observations and the small model error correction has little effect on orbit determination. However, the predicted orbit depends entirely on the accuracy of the dynamic models. Thus, a small model error is gradually highlighted in the orbit prediction. Therefore, the differences of the predicted orbits are more significant than the observed orbits. In addition, the overlapping period of scheme 2 is in the predicted orbital arc, whereas the overlapping period of scheme 3 is in the observed orbital arc. The distance between the model correction position and the predicted orbits of scheme 3 is greater than scheme 2. Therefore, the differences of the predicted orbits obtained by scheme 3 are bigger than scheme 2.

Furthermore, comparison of Figs. 15 and 17 reveals that the relationship between the size of the maximum difference of the shadow factor and the size of the orbital difference is not obvious. Considering the orbital integral step is 60 s in the orbit determination solution, the cumulative differences of the shadow factors at the orbital integral epochs in every overlapping period are shown in Fig. 18.

It can be seen from the comparison of Figs. 17 and 18 that due to the influence of the error of orbit determination, the relationship between the difference of orbital accuracy and the cumulative differences of the shadow factors at the orbital integral epochs in the overlapping period is not one to one correspondence. However, they satisfy the

basic correspondence relationship, i.e., the Cumulative differences of the shadow factors at the orbital integral epochs in the overlapping period is larger, the impact on the accuracy of orbit determination is usually larger. This is mainly because the perturbation forces in the orbital integral method are estimated according to the integral step. The differences of the orbit determination solutions obtained by the different dynamic models are caused mainly by the differences of the different dynamic models at the orbital integral epoch. Moreover, the differences of the different dynamic models at epochs that are not orbital integral epochs have no effect on the orbit determination solution.

#### 4.4. Comparison with IGS final orbit product

To analyze the improvement of the refined shadow function model on the accuracy of orbit determination, the orbit determination results of the three schemes discussed in Section 4.3 were compared with the IGS final orbit products. The orbital root mean square (RMS) comparisons of the three schemes are shown in Figs. 19–21.

It can be seen from Figs. 19–21 that with reference to the IGS final orbit products, the RMS differences of the observed orbits obtained separately using the original and refined models are small but that the RMS differences of the predicted orbits are large. This finding is consistent with Section 4.3. However, the results of the orbit determination solutions obtained using the refined shadow function model are not all improved. This is mainly because, although the models and strategies of orbit determination data processing in this paper are as far as possible consis-

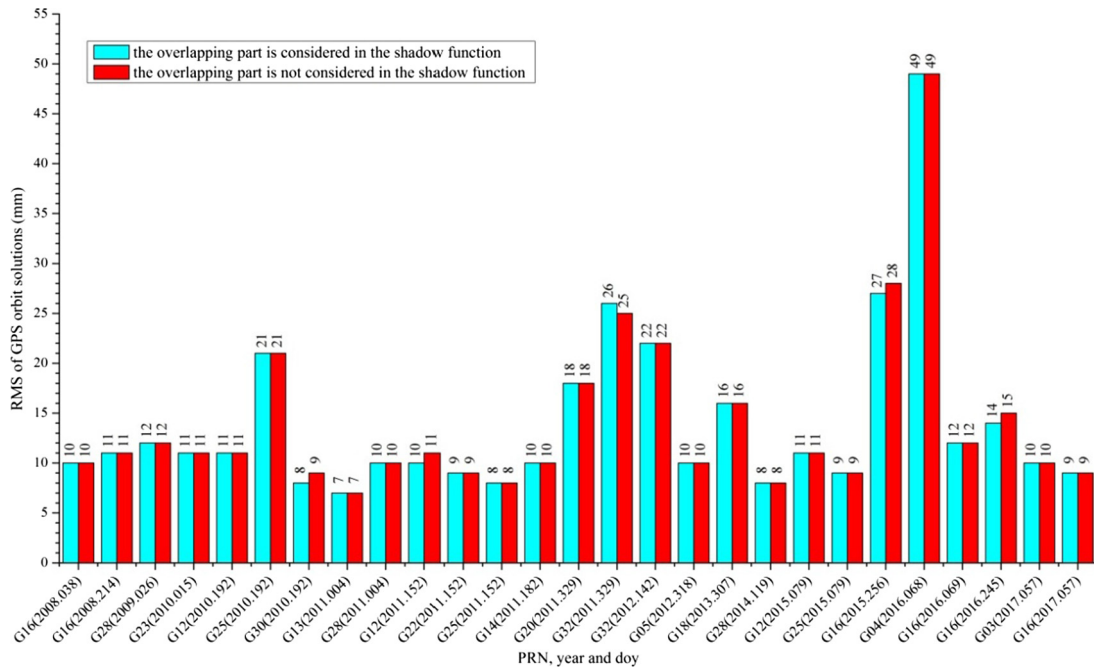


Fig. 19. Comparison between the observed orbits of the overlapping day and the IGS final orbit products.

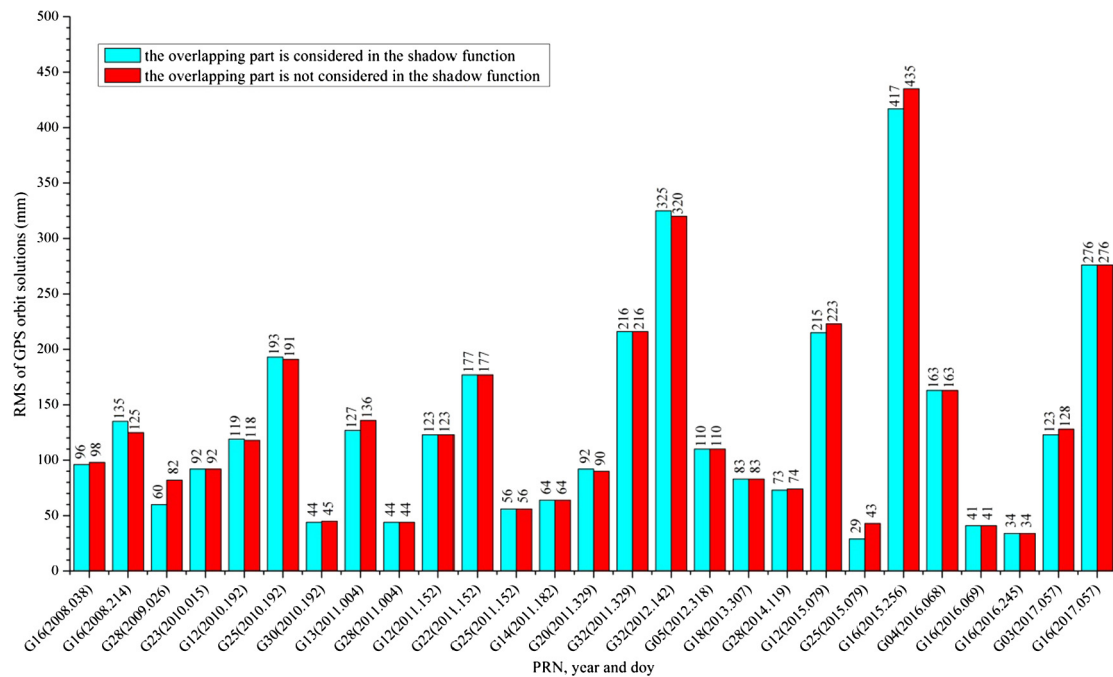


Fig. 20. Comparison between the predicted orbits of the overlapping day and the IGS final orbit products.

tent with those of the IGS final orbit product solutions, some models and strategies are different. Furthermore, accounting for the overlap of the shadows of the Earth and the Moon might not be considered in the shadow function model of the IGS final orbit product. Based on the above factors and with reference to the IGS final orbit products, the improvement of the refined shadow function model on the accuracy of orbit determination is not significant.

#### 4.5. Comparison with overlapping arc

To analyze the improvement of the refined shadow function model on the accuracy of orbit determination based on the same models and strategies of orbit determination data processing, the overlapping arcs were used to evaluate the GPS orbit determination solutions obtained separately using the original and refined models. The following two schemes were used and the illustration is shown in Fig. 22.

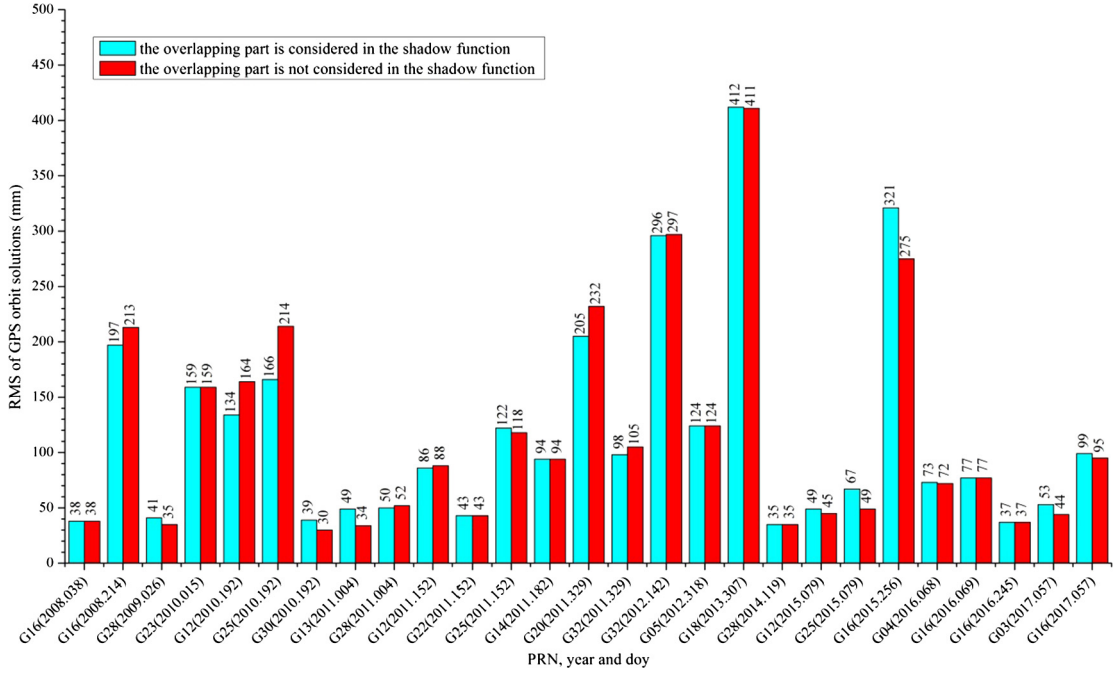


Fig. 21. Comparison between the predicted orbits of the day after the overlapping day and the IGS final orbit products.

Scheme 4: the three-day GPS observation data from the day before the overlapping day to the day after the overlapping day were used to obtain two consecutive two-day observed orbit solutions. The orbit of the second day in the first two-day solution was compared with that of the first day in the second two-day solution.

Scheme 5: the observed orbits of the day before the overlapping day were calculated and predicted orbits predicted for the overlapping day. The predicted orbits were compared with the observed orbits of the overlapping day.

The orbital RMS comparisons of schemes 4 and 5 are shown in Figs. 23 and 24, respectively.

It can be seen from Figs. 23 and 24 that the overlapping RMS differences of the observed orbits obtained separately using the original and refined models are small but that the overlapping RMS differences of the predicted orbits are large. This finding is consistent with Sections 4.3 and 4.4. However, unlike Section 4.4, the refined shadow function model is shown effective at improving the overlapping accuracy of the predicted orbit. The overlapping accuracy of 13 arcs in the 15 predicted orbital arcs which have differences is improved, i.e., an improvement rate of 86.7%. This is mainly because, based on the same models and strategies of orbit determination data processing, the refined shadow function model is more helpful to improve the self-consistency of the orbit determination. The actual orbit

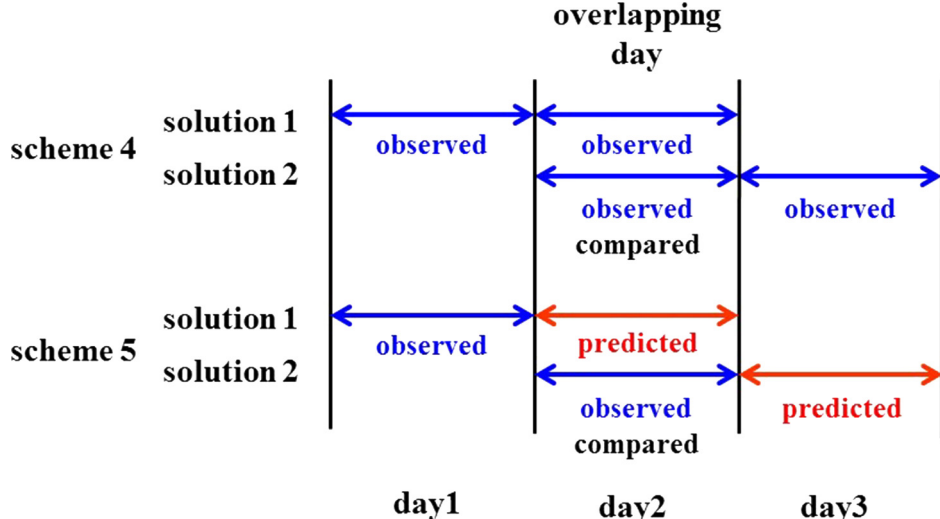


Fig. 22. Illustration of scheme4 and scheme 5.

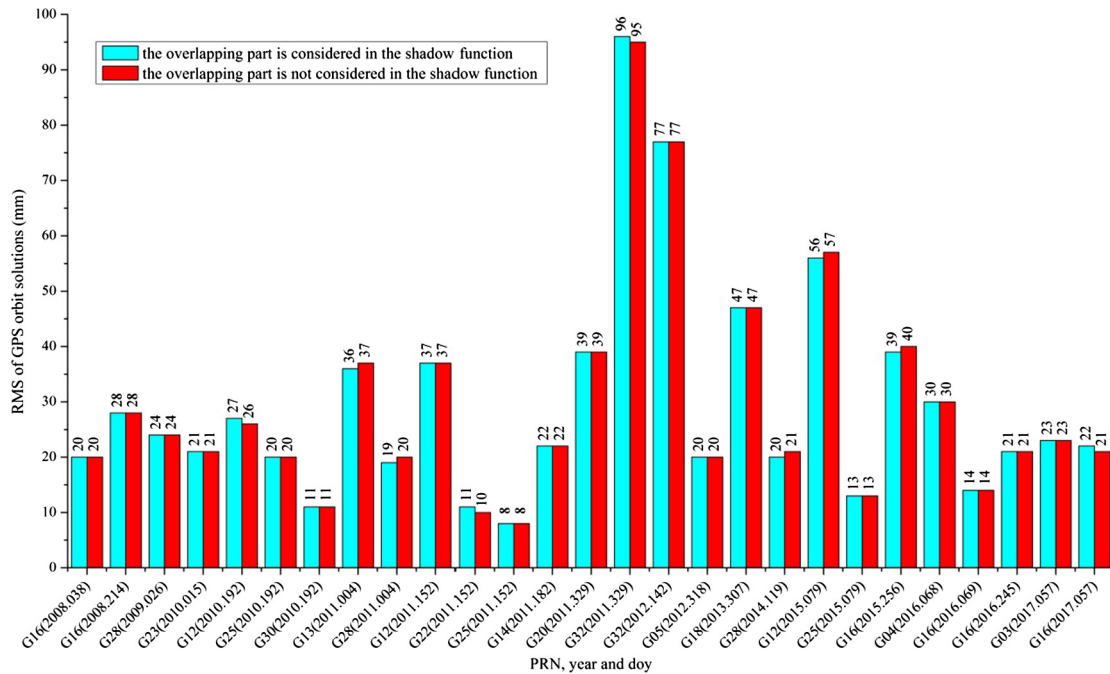


Fig. 23. Comparison of the overlapping arcs of the observed orbits.

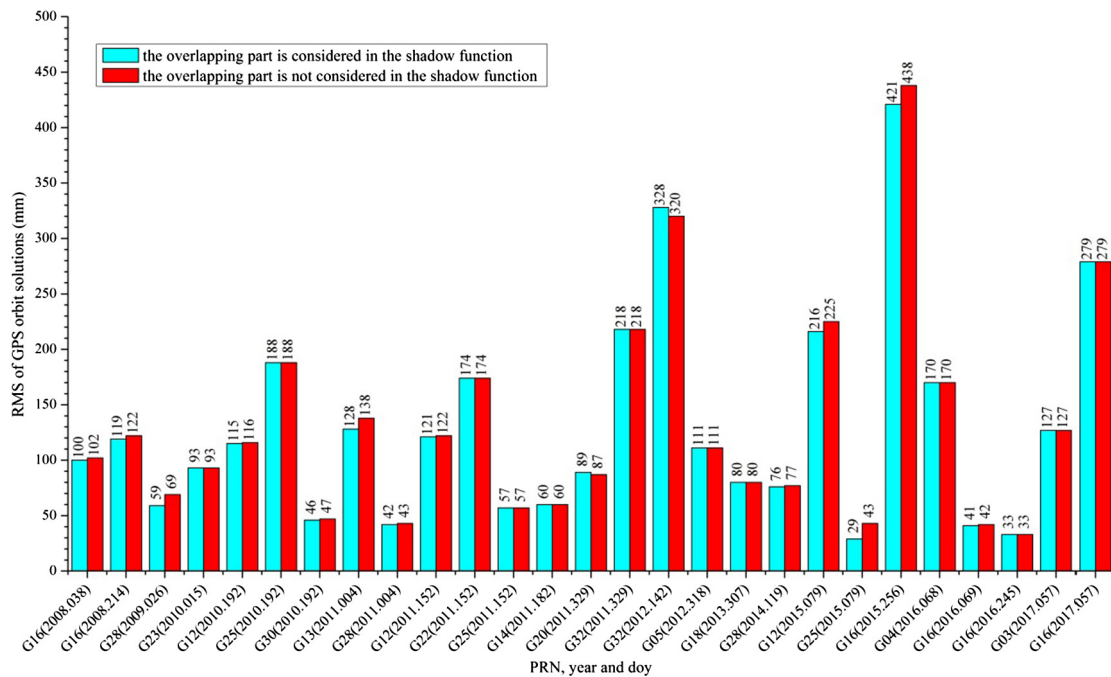


Fig. 24. Comparison of the overlapping arcs of the predicted orbits.

results also show that the refined shadow function model presented in this paper can improve the accuracy of orbit determination when a satellite enters the area of overlapping shadows of the Earth and the Moon.

## 5. Conclusions

To improve the accuracy of orbit determination when a satellite enters the area of overlapping shadows of the

Earth and the Moon, a refined shadow function model, based on the original shadow function model, has been presented in detail in this paper. The orbits of GPS satellites over nearly 10 years were analyzed using both the original and refined models. First, the periods during which the GPS satellites passed through the overlapping shadows were selected. Second, the differences between the original and refined shadow function models in every overlapping period were analyzed. Third, the improvement of the

refined shadow function model on the accuracy of orbit determination was analyzed. The specific conclusions of this paper are as follows:

- (1) During the study period (nearly 10 years), GPS satellites enter the area of overlapping shadows of the Earth and the Moon 27 times. The occurrence frequency of the satellites in the B orbital plane is high. The maximum duration of the passage of a satellite through the overlapping area in one day is 474 s. The maximum impact of the refined shadow function model on the solar radiation pressure perturbation is nearly 1/3 of the solar radiation pressure perturbation.
- (2) Affected by observation constraints, the refined shadow function model has little influence on observed orbits; however, it has considerable influence on predicted orbits. The maximum difference in a 24-h predicted orbit is 46 mm. For the same overlapping period, the greater the distance between the model correction position and the predicted orbital arc, the greater the impact of the refined shadow function model on the orbit determination solution.
- (3) The impact of the refined shadow function model on the accuracy of orbit determination is jointly decided by the value of the shadow factor and the number of orbital integral epochs in overlapping period. The Cumulative differences of the shadow factors at the orbital integral epochs in the overlapping period is larger, the impact of the refined shadow function model on the accuracy of orbit determination is usually larger.
- (4) Affected by the different models and strategies of orbit determination data processing, with reference to the IGS final orbit product, the improvement of orbital accuracy obtained by the refined shadow function model is not significant. However, based on the same models and strategies of orbit determination data processing, the improvement of orbital overlapping accuracy obtained by the refined shadow function model is significant, with an improvement rate of 86.7% for multiple predicted orbit solutions.
- (5) The IGS products are used to determine the periods during which the GPS satellites pass through the overlapping shadows of the Earth and the Moon. Satellites not provided in the IGS product are not analyzed. Therefore, there may be the rest of the period that the GPS satellites enter the overlapping part of the shadows of the Earth and the Moon. Furthermore, the refined shadow function model has little influence on orbit determination. The orbit determination accuracy of BeiDou satellite navigation system (BDS), Global Navigation Satellite System (GLONASS), Galileo satellite navigation system (Galileo), and other navigation systems is lower than that of

GPS; therefore, only GPS satellites are analyzed here. The improvement of the refined shadow function model on orbit determination of other navigation systems can be analyzed once the accuracy of orbit determination of other navigation systems is improved.

## Acknowledgments

This work was supported partly by the Chinese Academy of Sciences (CAS) program of “Western Youth Scholar” (Grant No.: Y712YR4701), the Program of National Natural Science Foundation of China (Grant Nos.: 41504006, 41674034), National Key Research and Development Plan of China (Grant No.: 2016YFB0501804) and Chinese Academy of Sciences (CAS) programs of “Pioneer Hundred Talents” and “The Frontier Science Research Project” (Grant No.: QYZDB-SSW-DQC028). The authors gratefully acknowledge the supports of Prof. Yang Yuanxi, Prof. Zhang Qin and Prof. Ge Maorong for their constructive suggestions. We also thank the IGS and iGMAS authorities for providing the data for this study.

## References

- Beutler, G., Brockmann, E., Gurtner, W., Hugentobler, U., Mervart, L., Rothacher, M., Verdun, A., 1994. Extended orbit modeling techniques at the CODE processing center of the International GPS Service for Geodynamics (IGS): theory and initial results. *Manuscripta Geodaetica*. 19, 367–386.
- Chen, L.C., 2007. How navigation satellite orbit numerical integration affected by shadow model and its correcting methods. *Geomatics Informat. Sci. Wuhan Univ.* 32 (5), 450–453.
- Dai, X.L., 2016. Real-Time Precise GNSS Satellite Orbit Determination Using the SRIF Method: Theory and Implementation. Wuhan University, China, Wuhan.
- Ding, J., Qu, F., Wei, Z.B., Li, Q., 2010. Calculating and analysis of satellite umbra based on Cartesian coordinate. *Sci. Surv. Mapp.* 35 (1), 39–40.
- Dow, J.M., Neilan, R.E., Rizos, C., 2009. The international GNSS service in a changing landscape of global navigation satellite systems. *J. Geod.* 83, 191–198.
- Du, L., Zhou, P.Y., Fang, S.C., Liu, Z.J., Guo, R., 2016. Satellite Shadow Modeling and Algorithm of Satellite Shadow Parameters for GNSS. *Acta Geodaet. Cartograph. Sin.* 45 (11), 1270–1277.
- Forste, C., Bruinsma, S., Shakoor, R., Marty, J.C., Flechtner, F., Abrikosov, O., Dahle, C., Lemoine, J.M., Neumayer, H., Biancale, R., Barthelmes, F., Konig, R., Balmino, G., 2011. EIGEN-6 – A new combined global gravity field model including GOCE data from the collaboration of GFZ-Potsdam and GRGS-Toulouse. *Arch. Gen. Psychiatry* 36 (6), 720–720.
- He, L.N., Ge, M.R., Wang, J.X., Wickert, J., Schuh, H., 2013. Experimental study on the precise orbit determination of the BeiDou navigation satellite system. *Sensors* 13, 2911–2928.
- Lyard, F., Lefevre, F., Letellier, T., Francis, O., 2006. Modelling the global ocean tides: modern insights from fes2004. *Ocean Dyn.* 56 (5–6), 394–415.
- Lou, Y.D., Liu, Y., Shi, C., Yao, X.G., Zheng, F., 2014. Precise orbit determination of BeiDou constellation based on BETS and MGEX network. *Sci. Rep.* 4, 4692.

- Mao, Y., Song, X.Y., Jia, X.L., Wu, X.B., 2014. Earth eclipse status analysis of beidou navigation satellites. *Acta Geodaet. Cartograph. Sin.* 4, 353–359.
- Montenbruck, O., Gill, E., 2000. Satellite Orbit Models, Methods and Applications. Springer-Verlag, Berlin Heidelberg.
- Oraevskii, V.N., Kuznetsov, S.N., Malyshev, V.V., Usachov, V.E., Tychinskii, Y.D., 2004. A study of a possible method of observing solar eclipses from satellite orbits. *Cosm. Res.* 42 (1), 23–31.
- Petit, G., Luzum, B., 2010. IERS conventions, IERS Technical Note No. 36. Verlag des Bundesamts für Kartographie und Geodäsie, Frankfurt am Main.
- Srivastava, V.K., Kumar, J., Kulshrestha, S., Srivastava, A., Bhaskar, M.K., Kushvah, B.S., Shiggavi, P., Vallado, D.A., 2015a. Lunar shadow eclipse prediction models for the earth orbiting spacecraft: comparison and application to LEO and GEO spacecrafat. *Acta Astronautica*. 110, 206–213.
- Srivastava, V.K., Yadav, S.M., Ashutosh, Kumar, J., Kushvah, B.S., Ramakrishna, B.N., Ekambaram, P., 2015b. Earth conical shadow modeling for LEO satellite using reference frame transformation technique: a comparative study with existing earth conical shadow models. *Astron. Comput.* 9 (9), 34–39.
- Standish, E.M., 1998. The JPL Planetary and Lunar Ephemerides DE402/LE402. *JPL IOM* 312. F-98-048.
- Tu, R., Ge, M.R., Zhang, H.P., Huang, G.W., 2013a. The realization and convergence analysis of combined PPP based on raw observation. *Adv. Space Res.* 52, 211–221.
- Tu, R., Zhang, H.P., Ge, M.R., Huang, G.W., 2013b. A real-time ionospheric model based on GNSS Precise Point Positioning. *Adv. Space Res.* 52, 1125–1134.
- Zhang, R., 2013. The Research and Program Design of GPS Satellite Orbit Determination Based on Ground Reference Station Observation. Chang'an University, Xi'an, China.
- Zhang, R., Zhang, Q., Huang, G.W., Wang, L., Qu, W., 2015. Impact of tracking station distribution structure on BeiDou satellite orbit determination. *Adv. Space Res.* 56 (10), 2177–2187.